Journal of Magnetic Resonance **150,** 17–25 (2001)
doi:10.1006/jmre.2001.2304, available online at http://www.idealibrary.com on IDEAL®

The Effects of Slice-Selective Excitation/Refocusing in Localized Spectral Editing with Gradient-Selected Double-Quantum Coherence Transfer

Hao Lei[1] and Jeffrey Dunn

Department of Diagnostic Radiology, Dartmouth Medical School, Hanover, New Hampshire 03755

Received August 31, 2000; published online April 2, 2001

Spectral editing using gradient-selected double-quantum filtering (DQF) with PRESS localization has been used for selective observation of metabolites *in vivo*. In previous studies using localized DQF sequences, it is generally assumed that the slice-selective pulses used in the sequence have no roles in coherence transfer, and do not interfere with DQF. To validate this assumption, the effects of slice-selective excitation/refocusing on DQF were investigated in DQF lactate editing sequences combined with PRESS localization. Contrary to the previous assumption, the results show that, due to chemical shift displacement artifact and *J* coupling, slice selection in DQF does interfere with coherence transfer, affecting both the accuracy of spatial localization and the detection sensitivity adversely. In the case of lactate editing, the effects of this interference can be accounted for simply by adjusting the strength of the slice-selection gradients and by using narrowband slice-selective refocusing pulses.

Key Words: **spectral editing; double-quantum coherence transfer; double-quantum filtering; chemical shift displacement artifact; spatial localization.**

INTRODUCTION

Severe spectral overlap and interference from lipid and water signals often limit the usefulness of ^{1}H magnetic resonance spectroscopy (MRS) *in vivo* (*1*). A family of spectral editing techniques has been developed to observe the resonance of *J*-coupled metabolites selectively and to suppress lipid/water signals (*2*, *3*). Among these, techniques using gradient-selected double-quantum filtering (DQF) provide a good compromise between lipid/water suppression, detection sensitivity for metabolite(s), and motion sensitivity, and show considerable promise for *in vivo* application (*2–4*).

However, the routine use of DQF in practice is still hindered by technical limitations such as reduced detection sensitivity and poor understanding in combining DQF with spatial localization. Theoretically, only a fraction (i.e., 25–50%) of the signals from the target resonance can pass through a DQF sequence, and the signals passing through the sequence are attenuated further by mechanisms such as transverse relaxation, spin diffusion, *J* modulation, and RF pulse imperfection (*3*, *4*). For spatial localization, DQF has been combined with both methods using chemical shift imaging (CSI) and methods using slice selection (*4–19*). Because of the intrinsically reduced detection sensitivity of the DQF sequences and the large voxel matrix size needed in CSI to avoid intervoxel leakage, DQF with CSI often requires a long acquisition time that is undesirable for *in vivo* applications (*4–7*). Localization in DQF has also been achieved using slice-selection techniques, including stimulated-echo acquisition mode (STEAM) (*8*, *9*), volume-selective spectral editing (VOSING) (*10*), volume-selective refocusing (VSR) (*11*), spatial and chemical shift-encoded excitation (SPACE) (*12*), image-selected *in vivo* spectroscopy (ISIS) (*13*), longitudinal Hadamard encoding (*14*), and point-resolved spectroscopy (PRESS) (*15–19*). DQF with PRESS localization seems to be the most successful among these, and has been used to perform localized spectral editing for lactate (*15*), γ-aminobutyric acid (GABA) (*16*), glucose (*17*), glutathione (*18*), and glutamate (*19*) *in vivo*. The main reasons for its success are because the pulse sequence is simple, it achieves spatial localization in a single shot, and more importantly it is believed that PRESS localization does not introduce any further reduction in detection sensitivity.

All spatial localization techniques using slice selection suffer from the well-known chemical shift displacement artifact, and this has been investigated thoroughly in PRESS and PRESS-like sequences (*20–22*). In addition, homonuclear *J* coupling affects the accuracy of spatial localization for lactate in PRESS (*23*). In previous studies using localized DQF sequences with slice selection, it has generally been assumed that the slice-selective pulses have no roles in coherence transfer, and therefore that the spatial localization element of the sequence does not interfere with DQF. However, it was recently shown that the slice profile obtained by a slice-selective refocusing pulse in DQF with PRESS is different from that obtained by the same pulse in conventional PRESS (*24*). To clarify this observation and to further investigate the roles of slice-selective pulses in DQF, the effects of slice-selective excitation/refocusing on DQ coherence transfer have been investigated both theoretically and experimentally in DQF sequences with PRESS localization. It is shown here that, due to the chemical shift displacement artifact and

[1] To whom correspondence should be addressed at Department of Diagnostic Radiology, Dartmouth Medical School, HB 7786, Vail 709, Hanover, NH 03755. Fax: (603) 650-1717. E-mail: Hao.Lei@dartmouth.edu.

1090-7807/01 $35.00

J coupling of the edited spin(s), slice-selective excitation/refocusing in DQF interferes with coherence transfer within the region of interest (ROI). The consequences of this interference and their solutions are also discussed.

THEORY

Figure 1 shows two commonly used DQF sequences with PRESS localization. The first 90° pulse and two 180° pulses in these sequences are slice selective to achieve three-dimensional spatial localization (*15–19*). Compared to sequence a, sequence b has an extra hard 180° pulse inserted in the middle of the DQ evolution period (t_1).

Let us consider the sequence shown in Fig. 1a first. It is well known that spatial localization obtained by slice-selective excitation/refocusing depends on the chemical shift of the resonance observed. For instance, for a weakly coupled two-spin-1/2 system (IS) with a frequency difference ω_{IS} between the two spins, the center of the slice selected by a slice-selective pulse for spin S is shifted relative to that for spin I by an amount

$$\Delta r = \frac{|\omega_{IS}|}{\delta} r, \qquad [1]$$

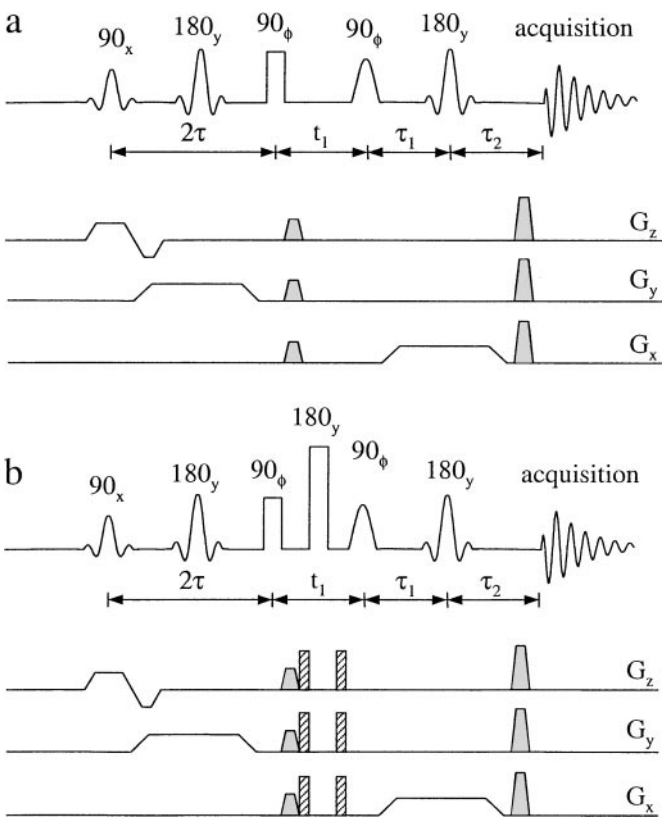

FIG. 1. Pulse sequences for spectral editing using double-quantum coherence transfer and PRESS spatial localization.

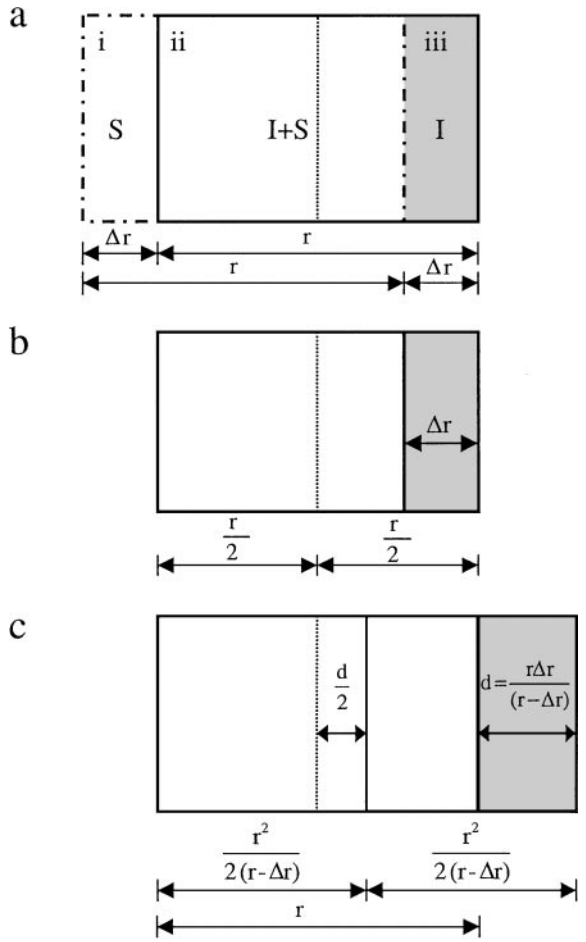

FIG. 2. Schematic representations of chemical shift-induced spatial displacement (a). Because of the chemical shift-induced spatial displacement and *J* coupling, calculating the strength of the slice-selective gradient and the frequency offset of the slice-selective pulse in double-quantum filtering (DQF) with PRESS localization (c) is different from that in normal PRESS (b) in order to obtain the same region of interest. r is the slice thickness of the region of interest, and Δr is the chemical shift-induced spatial displacement.

where r is the slice thickness, and δ ($\delta > |\omega_{IS}|$) is the bandwidth of the slice-selective pulse. Figure 2a shows a schematic representation of the chemical shift-induced spatial displacement. Suppose that the carrier frequency of the slice-selective pulse is set on resonance for I and the open area (i.e., region ii and region iii combined) is the desired ROI. Because the resonance frequency of S differs from that of I, the area in which S is selected by the pulse in the presence of a slice-selective gradient (i.e., region i and region ii combined) is shifted by Δr relative to the desired ROI. Note that both I and S are selected in region ii, while only S is selected in region i and only I is selected in region iii.

For the DQF element of the sequence without considering the pulses to be slice selective, antiphase coherence is generated during the DQ creation period (2τ) and is then converted into DQ coherence by the second 90° pulse. After t_1, the third 90° pulse (i.e., the DQ read pulse) converts the DQ coherence

back into single-quantum (SQ) coherence which is then detected at the end of the detection period ($\tau_1 + \tau_2$). When I is edited, the frequency of all the RF pulses in the sequence is set on resonance for I, except for the DQ read pulse for which a frequency-selective pulse with a frequency set on resonance for S is usually used to increase the intrinsic detection sensitivity (*3*). Using a product operator formalism in the spherical basis (*25*), the coherence transfer pathways involving the DQ coherence ($\mathbf{I}_+\mathbf{S}_+$) and leading to observable signals of spin I ($\mathbf{I}_-$) are

$$\mathbf{I}_0 \overset{90^\circ}{\rightarrow} \mathbf{I}_- \overset{\tau}{\rightarrow} \mathbf{I}_-\mathbf{S}_0 \overset{180^\circ}{\rightarrow} \mathbf{I}_+\mathbf{S}_0 \overset{\tau}{\rightarrow} \overset{90^\circ}{\rightarrow} \mathbf{I}_+\mathbf{S}_+ \overset{t_1}{\rightarrow} \overset{90^\circ}{\rightarrow} \mathbf{I}_+\mathbf{S}_0 \overset{\tau_1}{\rightarrow} \overset{180^\circ}{\rightarrow} \mathbf{I}_-\mathbf{S}_0 \overset{\tau_2}{\rightarrow} \mathbf{I}_-$$

and

$$\mathbf{I}_0 \overset{90^\circ}{\rightarrow} \mathbf{I}_+ \overset{\tau}{\rightarrow} \mathbf{I}_+\mathbf{S}_0 \overset{180^\circ}{\rightarrow} \mathbf{I}_-\mathbf{S}_0 \overset{\tau}{\rightarrow} \overset{90^\circ}{\rightarrow} \mathbf{I}_+\mathbf{S}_+ \overset{t_1}{\rightarrow} \overset{90^\circ}{\rightarrow} \mathbf{I}_+\mathbf{S}_0 \overset{\tau_1}{\rightarrow} \overset{180^\circ}{\rightarrow} \mathbf{I}_-\mathbf{S}_0 \overset{\tau_2}{\rightarrow} \mathbf{I}_-,$$

where $\mathbf{I}_0$ and $\mathbf{S}_0$ represent the longitudinal magnetization of I and S, respectively, and $\mathbf{I}_-\mathbf{S}_0$ and $\mathbf{I}_+\mathbf{S}_0$ represent the antiphase coherence.

Now consider the effects on DQ coherence transfer of making the pulses slice selective. The first 90° pulse converts $\mathbf{I}_0$ and $\mathbf{S}_0$ into SQ coherence. Because evolution of the SQ coherence of S in the subsequent coherence transfer steps does not lead to any observable signal of I, the chemical shift displacement artifact caused by this pulse will have no effects on the final results and thus can be ignored. The function of the two 180° pulses in the sequence is to interchange $\mathbf{I}_+\mathbf{S}_0$ and $\mathbf{I}_-\mathbf{S}_0$. To obtain perfect conversion from one to the other, the same 180° pulse should act as a perfect refocusing pulse for I and simultaneously as a perfect inversion pulse for S. However, this will obviously not be the case in practice. When no slice-selective gradient is applied, a real 180° pulse converts $\mathbf{I}_+\mathbf{S}_0$ into $\mathbf{I}_-\mathbf{S}_0$ with a conversion efficiency factor which is determined by experimental parameters such as the length and the RF power of the pulse as well as the properties of the spin system such as ω_{IS} (*24*). In the presence of a slice-selective gradient, the same 180° pulse refocuses I and inverts S in slices that are displaced from each other by Δr (Fig. 2a), and therefore coherence transfer in different parts of the ROI will be different. Consider the effects of making the second 180° pulse in Fig. 1a slice selective. In region ii of Fig 2a, I is refocused and simultaneously S is inverted, allowing normal coherence transfer:

$$\mathbf{I}_+\mathbf{S}_0 \overset{\tau_1}{\rightarrow} \overset{180^\circ_{I+S}}{\rightarrow} \overset{\tau_2}{\rightarrow} \sin[(\tau_1 + \tau_2)\pi J]\mathbf{I}_-. \qquad [2]$$

In region iii, I is refocused, but S is not inverted. Coherence transfer in this region is

$$\mathbf{I}_+\mathbf{S}_0 \overset{\tau_1}{\rightarrow} \overset{180^\circ_{I}}{\rightarrow} \overset{\tau_2}{\rightarrow} \sin[(\tau_1 - \tau_2)\pi J]\mathbf{I}_-, \qquad [3]$$

where J is the scalar coupling constant between I and S, and the subscripts I and S in Eqs. [2] and [3] represent I spins and S spins, respectively. In region i, S is inverted and I is not refocused so that the antiphase coherence will be dephased by the crusher gradients around the 180° pulse, and there will be no contribution from this region to the final signal observed. If $\tau_1 = \tau_2 = 1/4J$, no signal will be received from region iii (Eq. [3]), and consequently the slice observed will have reduced thickness r-Δr and the center of the slice will be shifted by $\Delta r/2$ compared to the desired ROI which is assumed to be the slice observed for nonedited spins by the same pulse in a normal PRESS experiment. In some of the previous studies (*15*), τ_1 and τ_2 were set to $\tau - t_1$ and $\tau + t_1$ respectively to simultaneously refocus the coherence transfer echo and the B_0 inhomogeneity experienced by the DQ coherence during the t_1 period. In this case, signal from region iii will be 180° out of phase with that from region ii (Eq. [3]), and thus the signals from these two regions will cancel each other. Assuming that the distribution of the spins is homogeneous and an integrated signal intensity of unity from the desired ROI, the signal intensity detected experimentally, Int(t_1), will be,

$$\mathrm{Int}(t_1) = \left[\left(1 - \frac{|\omega_{IS}|}{\delta}\right) - \frac{|\omega_{IS}|}{\delta}\sin(2\pi J t_1)\right] \times \cos^2(\pi J t_1). \qquad [4]$$

The profile of the slice actually selected will be irregular because of cancellation between the signals from the two regions. A similar analysis can be also applied to the first 180° pulse. Because the DQ creation period is always symmetrical with respect to the center of the first 180° pulse, no antiphase coherence will be generated in the Δr at the end of 2τ (Eq. [3]) and subsequent coherence transfer in this region will result in no observable signal.

The simplest way to ameliorate this problem is to use slice-selective 180° pulses with high bandwidths to reduce the size of Δr relative to r. However, pulses with high bandwidths require high RF power which can be limited by the RF amplifier. The problem can also be solved by adjusting the strength of the slice-selective gradient (G) and the frequency offset of the pulse ($\Delta\omega$) to select a slice that has the same slice thickness and is at the same localization as the desired ROI. Figures 2b and 2c illustrate how this can be done experimentally. Normally, when a slice-selective pulse with bandwidth δ ($\delta > |\omega_{IS}|$) is used to select a slice of thickness r and with a spatial offset D, G and $\Delta\omega$ are given by

$$G = \frac{\delta}{r} \qquad [5]$$

$$\Delta\omega = \frac{\delta \times D}{r}. \qquad [6]$$

However, as discussed above, this combination of G and $\Delta\omega$ will actually select a slice with a reduced thickness and with a shifted center when used in DQF with PRESS (Fig. 2b). If G is calculated using

$$G = \frac{\delta - |\omega_{IS}|}{r}, \quad [7]$$

a slice with a thickness r_{new} will be selected in normal PRESS,

$$r_{new} = \frac{\delta r}{\delta - |\omega_{IS}|} = \frac{r^2}{(r - \Delta r)}. \quad [8]$$

Provided that there is no contribution from the Δr region to the observed signal, the slice thickness obtained in DQF with PRESS will be (Fig. 2c)

$$r_{new} \times \left(1 - \frac{|\omega_{IS}|}{\delta}\right) = r. \quad [9]$$

In order for the slice actually selected to correspond to the desired ROI (Fig. 2c), the offset of the pulse must be determined using

$$\Delta\omega = \frac{(\delta - |\omega_{IS}|) \times D}{r} + \frac{\omega_{IS}}{2}. \quad [10]$$

The above method works well for the first 180° pulse. However, to be able to use Eqs. [7] and [10] to calculate G and $\Delta\omega$ for the second 180° pulse, $\tau_1 = \tau_2$ is required. By setting $\tau_1 = \tau_2$, however, the B_0 inhomogeneity experienced by the DQ coherence during the t_1 period will not be refocused, affecting both the intensity and the lineshape of the final signal observed (*3*). The sequence shown in Fig. 1b is a sequence in which $\tau_1 = \tau_2$ and simultaneously the B_0 inhomogeneity is refocused (*3, 16, 17*). The extra hard 180° pulse at the center of t_1 refocuses both chemical shift and B_0 inhomogeneity experienced by I and S during this period. Because no cancellation of signals occurs in this sequence, in theory it should give higher detection sensitivity than the sequence shown in Fig. 1a. However, in practice, because more RF pulse and crusher gradients are involved, this sequence is often more susceptible to imperfection in RF power calibration, breaking through of unwanted coherence transfer pathways, and formation of gradient echoes.

In cases where ω_{IS} is relatively large (i.e., in the order of several hundred hertz), the localization problem for the second 180° pulse in the sequence shown in Fig. 1a can also be solved by using a narrowband pulse with $\delta < |\omega_{IS}|$. Such a pulse refocuses I uniformly throughout the desired ROI, but does not invert S. As long as the DQ detection periods are asymmetrical around the 180° pulse, refocusing in this way will generate a signal with an integrated intensity which can be described by Eq. [11]

$$\text{Int}(t_1) = -\sin(2\pi J t_1)\cos^2(\pi J t_1). \quad [11]$$

Under these conditions, G and $\Delta\omega$ should be calculated normally using Eqs. [5] and [6].

EXPERIMENTAL

All experiments were carried out on a Varian ^{UNITY}INOVA console connected to a 7-T/20-cm Magnex magnet equipped with actively shielded gradients. A Varian quadrature coil with a diameter of 4 cm was used for both transmission and reception. All experiments were performed on a 1.2-cm-diameter cylindrical phantom containing 27 mM lactate solution in saline. Lactate-edited spectra were acquired with the sequences shown in Figs. 1a and 1b using a 10-ms single-lobe sinc pulse for the DQ read pulse, TR = 6.0 s, $2\tau = 72$ ms, a spectral bandwidth of 5000 Hz, 2048 data points, and 16 averages. For other pulses in the sequences, hard pulses were used unless otherwise specified. In the sequence shown in Fig. 1a, τ_1 and τ_2 were set to $\tau - t_1$ and $\tau + t_1$, respectively. In the sequence shown in Fig. 1b, $\tau_1 = \tau_2 = \tau$. The carrier frequency was set on resonance for the lactate methyl group, and the frequency of the read pulse was centered on the lactate methine resonance. The flip angles of all pulses were carefully calibrated. The orientation and the amplitude of all crusher gradients and coherence transfer pathway selection gradients were adjusted experimentally to maximize the efficiency of water suppression and to minimize the formation of gradient echoes.

The first set of four experiments was done without spatial localization, and three-lobe sinc pulses were used for 180° pulses. In the first experiment, the *normal* refocusing profiles of 1- and 2-ms sinc pulses were determined by acquiring water spectra using a double spin-echo sequence (TE1 = TE2 = 72 ms) as the frequency offset of the second 180° pulse was varied from −4000 (e.g., upfield) to 4000 Hz (e.g., downfield) relative to the resonance frequency of water. In the second experiment, lactate editing was performed using either 1- or 2-ms sinc pulses for both the first and the last 180° pulses as the frequency offset of the last 180° pulse was varied from −3000 to 3000 Hz with respect to the carrier frequency. $t_1 = 16$ ms. In the third experiment without spatial localization, a sinc pulse was used for either the first 180° pulse or the last 180° pulse, with a hard pulse used for the other 180° pulse(s). Lactate editing was performed as the length of the sinc pulse was varied from 1 to 8 ms in 0.5-ms increments, with $t_1 = 16$ ms. In the fourth experiment, a sinc pulse of either 1 or 6 ms was used for the last 180° pulse. Lactate editing was performed as t_1 was varied from 10 to 26 ms in 2-ms increments.

In the second set of experiments, lactate-edited spectra were acquired from a 10-mm slice located at the center of the magnet selected by using a slice-selective three-lobe sinc pulse for the last 180° pulse in the pulse sequence shown in Fig. 1a. The pulse length of the sinc refocusing pulse varied from 1 to 8 ms, and $t_1 = 16$ or 24 ms.

In the third set of experiments, lactate-edited spectra were acquired from a $20 \times 20 \times 10$-mm^3 voxel, with t_1 of either 16

or 24 ms. Three-lobe sinc pulses 1 ms long were used for the first 90° pulse and for the first 180° pulse. A three-lobe sinc pulse with a length of either 1 or 6 ms was used for the second slice-selective 180° pulse. The phase (ϕ) of the DQ creation pulse and the DQ read pulse was determined as described by Trabesinger *et al.* (*18*). For the first slice-selective 180° pulse, G and $\Delta\omega$ were calculated using Eqs. [7] and [10]. For the second slice-selective 180° pulse, G and $\Delta\omega$ were calculated using either Eqs. [7] and [10] or Eqs. [5] and [6].

Post-acquisition spectral processing in all cases included zero-filling the free induction decays to either 4096 or 8192 data points and applying a 2- to 5-Hz exponential line broadening. Spectra were phased individually to give a pure absorption lineshape and then corrected for baseline drifting. For quantification, the intensity of the lactate methyl signal was used when it could be confirmed that the linewidth remained constant throughout the experiment. Otherwise, the area under the edited lactate signal, derived using spectral deconvolution with a pure Lorentzian lineshape, was used.

A custom-written Fortran 77 program using a rotation matrix algorithm was used to evaluate the refocusing and inversion profiles of the sinc pulses numerically. Depending on the pulse length, the RF power used for simulation was such that a 180° flip angle was produced at the carrier frequency. The chemical shift difference and the J coupling constant between the lactate methyl group and the lactate methine group used for simulation were 832 and 7 Hz, respectively (*26*). When needed, the areas under the profile curves were calculated by a 1000-step numerical integration.

RESULTS

The dependence of the water signal intensity on the frequency offset of the second 180° pulse in the double spin-echo sequence is shown in Fig. 3a. For both 1- and 2-ms pulses, the profiles are symmetrical with respect to the resonance frequency of water and have shapes typically seen for sinc pulses. The refocusing bandwidths for 1- and 2-ms sinc pulses are 4400 and 2200 Hz, respectively. When used as the last 180° pulse in DQF lactate editing sequences, the refocusing profiles of the sinc pulses are remarkably different from those shown in Fig. 3a. In the sequence shown in Fig. 1b, the refocusing profiles have reduced

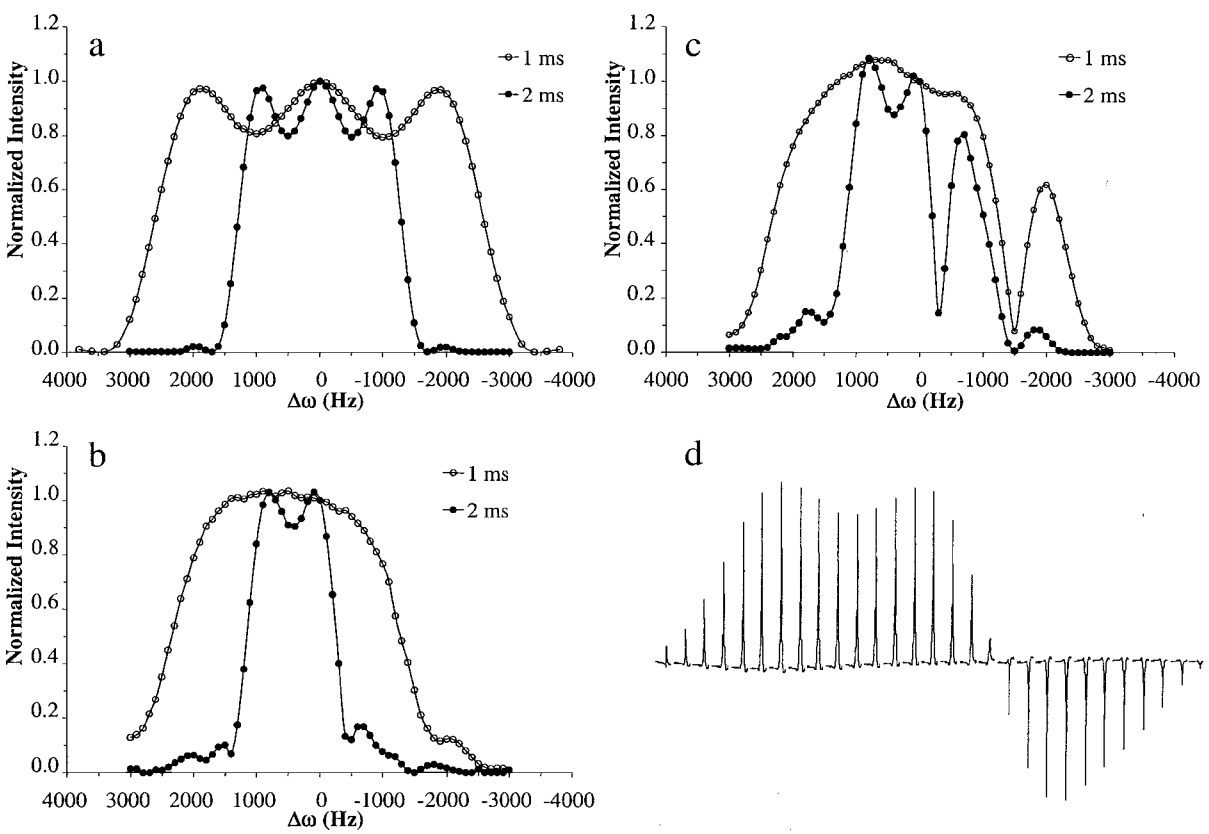

FIG. 3. The dependence of water signal intensity on the frequency offset of the last 180° pulse in a double spin-echo sequence (a). The dependence of edited lactate signal intensity on the frequency offset of the last 180° pulse in the pulse sequences shown Figs. 1b and 1a is shown in b and c, respectively. In a–c, open and closed circles represent the experimental data obtained using 1- and 2-ms three-lobe sinc 180° pulses, respectively. The solid lines connect data points. Panel d shows stacked spectra of an edited lactate methyl resonance acquired using the sequence shown in Fig. 1a, with a 2-ms sinc pulse used for the last 180° pulse whose frequency offset was varied between −1400 (rightmost) and 1400 Hz (leftmost) in 100-Hz increments.

bandwidths and are shifted downfield (Fig. 3b). In the sequence shown in Fig. 1a, the refocusing profiles of the sinc pulses are irregular in shape, with two components under each curve (Fig. 3c). The total bandwidth of the two components for each pulse is similar to the bandwidth for the same pulse when used in a double spin-echo experiment (Fig. 3a). The bandwidths of the upfield components are virtually the same, about 800 Hz, for the 1- and 2-ms pulses. The downfield components of the profiles resemble the profiles in Fig. 3b, and have higher signal intensity than the corresponding upfield components. Figure 3d shows stacked spectra of an edited lactate methyl resonance acquired using the sequence shown in Fig. 1a with a 2-ms sinc pulse used for the last 180° pulse. The frequency offset of the sinc pulse was varied between −1400 (rightmost) and 1400 Hz (leftmost) in 100-Hz increments. All spectra were scaled identically and had the same zero-order phase correction. A 180° phase reversal for the edited lactate signals occurs between −300 and −400 Hz, the frequency separating the two components of the profile curve of the pulse (Fig. 3c).

Figure 4a shows the dependence of the integrated lactate signal intensities on the lengths of the sinc refocusing pulses without spatial localization. The lactate signal intensities remained constant when the pulse lengths of the first 180° pulse in the sequence from Fig. 1a (closed circles), or the last 180° pulse in the sequence from Fig. 1b (open circles), were between 1 and 2 ms, declined when the pulses had lengths between 2 and 3 ms, and disappeared when the pulses were longer than 3 ms. When the sinc pulse was used as the second 180° pulse in the sequence from Fig. 1a (closed squares), the lactate signal intensities remained constant when the pulse length was between 1 and 2 ms, fluctuated when the pulse had a length between 2 and 5 ms, and became constant again when the pulse was longer than 5 ms. The solid line represents a numerical simulation for the data represented by the closed squares, and models the shape of the experimental curve well. The dashed lines connect data points. Figure 4b shows the dependence of the integrated lactate signal intensity on t_1 in the sequence shown in Fig. 1a when a sinc pulse of either 1 (closed circle) or 6 (open triangle) ms was used for the second 180° pulse. With the 1-ms refocusing pulse ($\delta = 4400$ Hz), the lactate signal intensity decreased monotonically with increasing t_1. With the 6-ms refocusing pulse ($\delta =$ 733 Hz), however, the lactate signal intensity increased with t_1 within the observed t_1 range, and reached a maximum at t_1 of 22–24 ms. The solid curves are theoretical predictions from Eqs. [4] and [11], and fit the shape of the experimental curves well.

Figure 5 shows the dependence of the integrated lactate signal intensity on the length of the last 180° in the sequence shown in Fig. 1a, which was used to achieve one-dimensional spatial localization. At $t_1 = 16$ ms, a 6-ms sinc pulse resulted in an integrated lactate intensity 12% higher than that obtained using a 1-ms sinc pulse. At $t_1 = 24$ ms, the increase was as high as 80%. The numerical simulations using Eqs. [4] and [11] models the basic features of the experimental data reasonably well.

Figure 6 shows lactate-edited spectra acquired from a $20 \times 20 \times 10$-mm^3 voxel and gives the integrated signal intensities (ISI) of the lactate peaks. The spectra shown in the left and right columns were acquired with t_1 of 16 and 24 ms, respectively. Spectra 6a to 6d were obtained using the sequence shown in Fig. 1a. Spectra 6a and 6b were obtained using a 6-ms sinc pulse for the second slice-selective refocusing pulse, while spectra 6c and 6d were obtained with a 1-ms refocusing pulse. Spectra 6e to 6h were acquired using the sequence shown in Fig. 1b

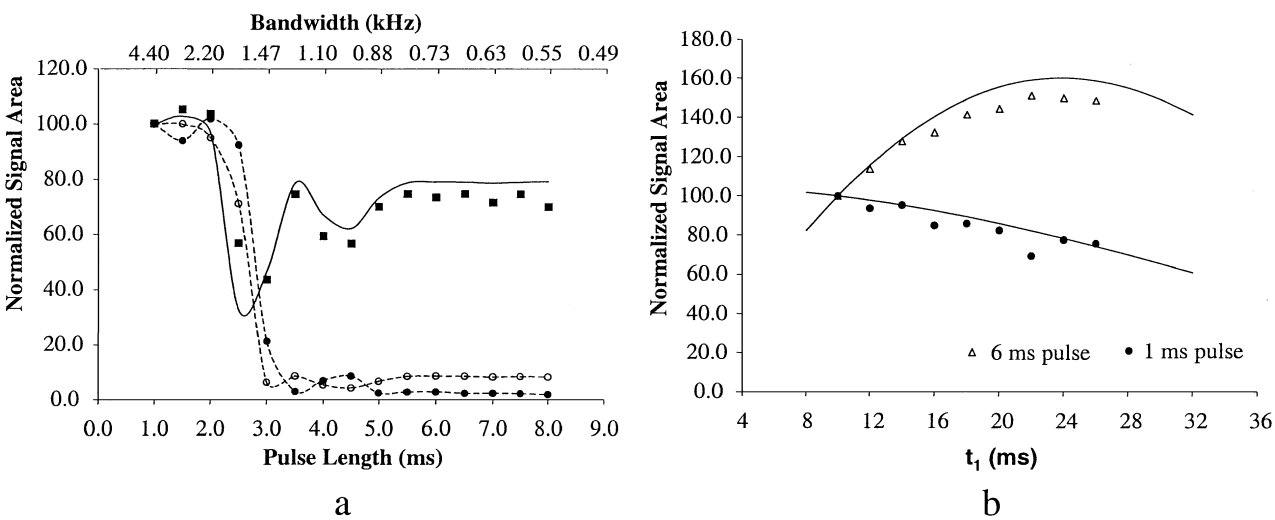

FIG. 4. The dependence of edited lactate signal intensity on the pulse lengths of the 180° pulses (a) and the duration of t_1 (b) without spatial localization. In a, open and closed circles represent the experiment data acquired when the pulse lengths of the last 180° pulse in the sequence shown in Fig. 1b and the first 180° pulse in the sequence shown in Fig. 1a were changed, respectively. Closed squares represent the experiment data acquired when the pulse lengths of the last 180° pulse in the sequence shown in Fig. 1a were changed, and the solid line represents a numerical simulation for these data. The dashed lines connect data points. In b, solid lines represent numerical simulation for the experimental data (open triangles and closed circles) using Eqs. [4] and [11].

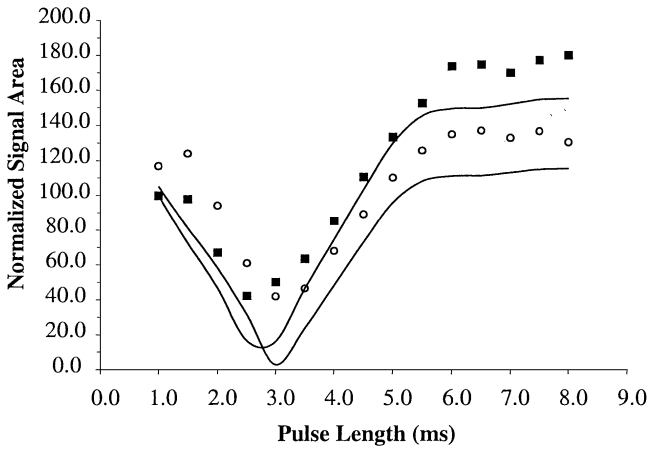

FIG. 5. The dependence of edited lactate signal intensity on the pulse length of the last 180° pulse in the sequence shown in Fig. 1a with one-dimensional spatial localization. Open circles and closed squares represent the experiment data acquired when the duration of t_1 was 16 and 24 ms, respectively. Solid lines represent numerical simulation for the experimental data using Eqs. [4] and [11].

with a second slice-selective refocusing pulse of 1 ms. G and $\Delta\omega$ of this pulse were determined using either Eqs. [7] and [10] (6g and 6h) or Eqs. [5] and [6] (6e and 6f). The edited lactate methyl signal is a singlet when the refocusing pulse refocuses the lactate methyl resonance only (6a and 6b), while all other spectra show a doublet signal. Spectrum 6b has the largest integrated signal intensity among all the spectra, about 40% higher than spectra 6c and 6e.

DISCUSSION

Gradient-selected DQF techniques acquire metabolite-edited spectrum in a single-shot with good lipid and water suppression, and thus are useful for *in vivo* MR spectroscopy (*3*). These techniques have been used successfully in a number of studies to observe cerebral metabolite *in vivo* (*15–19, 27*). However, two major technical problems have yet to be solved before the routine use of gradient-selected DQF in practice. First, as the cost for detecting metabolites selectively, the DQF sequences only observe coherence transfer pathways involving DQ coherence, which contribute only 25–50% of the total signals available. In practice, the observed signals are attenuated further by mechanisms such as transverse relaxation, spin diffusion, J modulation, and RF pulse imperfection (*4*). One way to improve detection sensitivity is to develop DQF sequences which recover full signals of the edited metabolite(s) (*4, 28*). However, these sequences require either phase cycling or add/subtraction of sequentially acquired spectra, and thus are susceptible to motion artifact and also are less efficient in water/lipid suppression, making them less useful for *in vivo* applications. Another way, probably also the most practical way, to ameliorate the detection sensitivity problem for the conventional DQF techniques is to identify and understand all the mechanisms that reduce the detection sensitivity experimentally. By doing so and by making technical improvements for each of them, it is possible to have an experimental detection sensitivity that is close to the theoretical maximum which, although reduced from full, will still make these editing techniques useful in practice. The second difficulty in using DQF

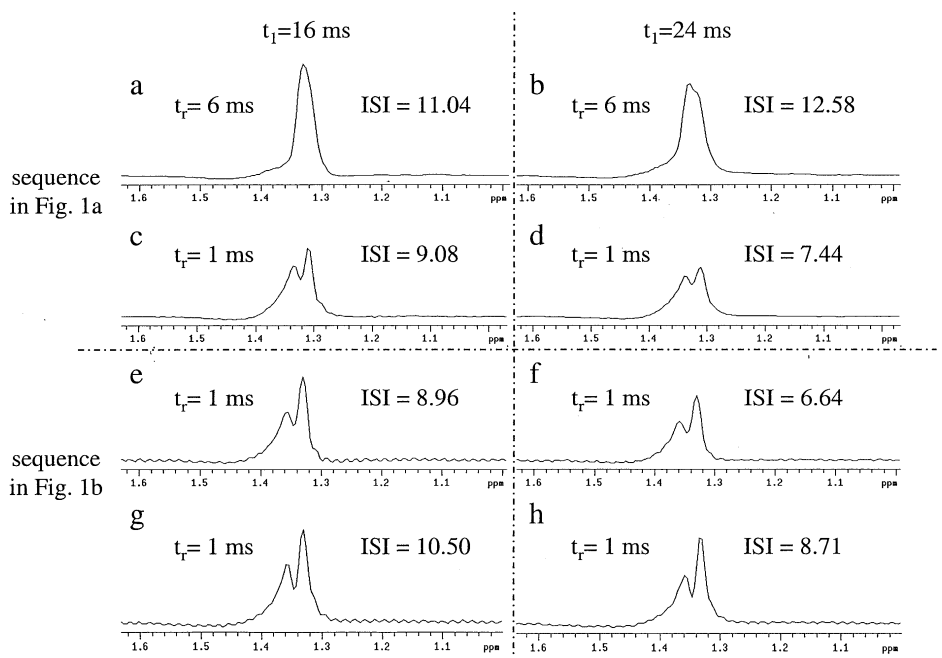

FIG. 6. Spectra and integrated signal intensities (ISI) of edited lactate methyl resonance acquired from a $20 \times 20 \times 10$-mm^3 voxel in a lactate-containing phantom using stated experimental settings. The effects of the selection of pulse sequences, t_1, the duration of the second slice-selective refocusing pulses (t_r), and the methods for calculating the strength of the slice-selective gradients on ISI are shown. See Results for detailed descriptions.

in vivo is to combine it with spatial localization, an essential element for all *in vivo* MRS. Most of the earlier developments in DQF sequences were done either without spatial localization or with spatial localization that either reduces the already-reduced detection sensitivity or compromises the motion sensitivity of the sequences (*8–14*).

DQF with single-shot PRESS localization has recently emerged as the most successful and practical spectral editing technique for *in vivo* applications (*15–19*). However, despite the success, two questions remain. First, is spatial localization achieved by PRESS in DQF sequences for a *J*-coupled metabolite the same as that achieved by normal PRESS for noncoupled metabolites? Second, does PRESS localization interfere with DQF in any way and impose any reduction in detection sensitivity for the edited metabolite(s)? To answer these two questions, the effects of slice-selective excitation and refocusing on DQ coherence transfer were investigated in this study. The results show that, due to the chemical shift displacement artifact and *J* coupling, slice-selective excitation/refocusing in DQF sequences does interfere with coherence transfer. If not accounted for, this interference will result in inaccuracy in spatial localization and a reduced detection sensitivity.

When a shaped pulse is used as a slice-selective pulse in DQF with PRESS localization, the frequency profile generated by the pulse is different from that observed in a simple PRESS experiment for observing noncoupled metabolites, and this is especially true for slice-selective refocusing pulses (Fig. 3). Instead of acting on SQ coherence as they do in normal PRESS for observing noncoupled metabolites, the two slice-selective refocusing pulses in DQF sequences with PRESS localization act on antiphase coherence that always involves two or more coupled spins with different chemical shifts. The RF pulses that are on resonance for one spin will be off resonance for other spin(s). Because of the off-resonance effects, refocusing of the antiphase coherence will be inhomogeneously across the ROI. Through *J*-coupling-induced coherence evolution, this in turn causes different coherence transfer in different parts of the ROI. The final manifestation of this effect is that the signal from one part of the ROI vanishes (Fig. 3b) or cancels with the signal from another part (Figs. 3c and 3d), resulting in a difference between the volume actually selected experimentally and the target ROI and therefore inaccuracy in spatial localization and a reduced detection sensitivity.

The interference between DQF and slice-selective refocusing is further demonstrated in Fig. 4 and Fig. 5. Even without slice-selective gradients, the lengths of the refocusing pulses affect the observed intensities of the edited lactate signals (Fig. 4a). This is a result of bandwidth of the refocusing pulse and off-resonance effects mentioned above. When the refocusing pulse is set on resonance for the lactate methyl group, it will be off resonance for the lactate methine group. Depending on the bandwidth and therefore the length of the refocusing pulse, the lactate methine group is either inverted completely (e.g., pulse length less than 2 ms) or incompletely (e.g., pulse length between 2 and 5.5 ms), or not inverted at all (e.g., pulse length longer than 5.5 ms). The refocusing patterns of the lactate antiphase coherence are therefore different with refocusing pulses of different lengths. Through coherence transfer, the eventual manifest is the dependence of the signal intensity on the refocusing pulse length observed in Fig. 4a. Similarly the lengths of the refocusing pulses affect the intensities of the edited lactate signals in the presence of a slice-selective gradient (Fig. 5). In both cases, theoretical simulations agree with experimental data reasonably well, and the noticeable discrepancy between the two could be due to B_1 inhomogeneity of the RF coil, other imperfections of the pulses, and coherence transfer during the pulses which is not considered in the theoretical simulation used in this study (*29*).

This study used DQF sequences with PRESS localization as examples. However, the results obtained can readily be extended to other localized DQF sequences using slice selection. By understanding the mechanisms underlying the interference between slice selection and DQF, it is possible to design localized DQF sequences with more accurate spatial localization and better detection sensitivities as shown in Fig. 6. Although the detection sensitivities obtained experimentally by using the conventional and the proposed experimental settings are not compared relative to the maximum theoretical detection sensitivity directly, it is clear from Fig. 6 that, by using the experimental settings proposed in this study for lactate editing (Fig. 6b), the detection sensitivity for lactate can be improved by as much as 40% compared to what is obtained when the conventional settings are used (Figs. 6c and 6e).

The exact interference pattern and the extent to which this interference affects the experimental outcome depend on the field strength and the RF pulses used, and on the spin system(s) of the metabolite(s) observed. For metabolites with complicated coupling systems such as glutamate and glutathione, analytical expressions that can be used to describe the interference quantitatively, such as Eqs. [4] and [11] in this study, are not always readily obtainable. Therefore, the simple solutions proposed in this study for lactate editing might not be applicable or sufficient in dealing with spectral editing for other metabolites. For a given pulse sequence and a given metabolite targeted for editing, another possible solution would be developing an algorithm that can be used to evaluate the performance of the sequence theoretically in terms of both the accuracy in spatial localization and the actual detection sensitivity (*19*). The results obtained from the evaluation could then be used either to optimize the pulse sequence before acquisition or to account for the experimental errors in data analysis after acquisition.

ACKNOWLEDGMENTS

Dr. J. J. H. Ackerman is thanked for bringing one of the key references to the author's attention. Dr. J. Peeling is thanked for reviewing the manuscript and his helpful suggestions.

REFERENCES

1. F. A. Howe, R. J. Maxwell, D. E. Saunders, M. M. Brown, and J. R. Griffiths, Proton spectroscopy in vivo, *Magn. Reson. Q.* **9,** 31 (1993).
2. P. S. Allen, R. B. Thompson, and A. H. Wilman, Metabolite-specific NMR spectroscopy in vivo, *NMR Biomed.* **10,** 435 (1997).
3. J. E. van Dijk, A. F. Mehlkopf, and W. M. Bovee, Comparison of double and zero quantum NMR editing techniques for in vivo use, *NMR Biomed.* **5,** 75 (1992).
4. Q. He, D. C. Shungu, P. C. van Zijl, Z. M. Bhujwalla, and J. D. Glickson, Single-scan *in vivo* lactate editing with complete lipid and water suppression by selective multiple-quantum-coherence transfer (Sel-MQC) with application to tumors, *J. Magn. Reson. B* **106,** 203 (1995).
5. Q. He, Z. M. Bhujwalla, and J. D. Glickson, Proton detection of choline and lactate in EMT6 tumors by spin-echo-enhanced selective multiple-quantum-coherence transfer, *J. Magn. Reson. B* **112,** 18 (1996).
6. R. E. Hurd and D. M. Freeman, Metabolite specific proton magnetic resonance imaging, *Pro. Natl. Acad. Sci. USA* **86,** 4402 (1989).
7. J. Shen, D. C. Shungu, and D. L. Rothman, In vivo chemical shift imaging of γ-aminobutyric acid in the human brain, *Magn. Reson. Med.* **41,** 35 (1999).
8. C. H. Sotak, D. M. Freeman, and R. E. Hurd, The unequivocal determination of *in vivo* lactic acid using two dimensional double-quantum coherence-transfer spectroscopy, *J. Magn. Reson.* **78,** 355 (1988).
9. C. H. Sotak and D. M. Freeman, A method for volume-localized lactate editing using zero-quantum coherence created in a stimulated-echo pulse sequence, *J. Magn. Reson.* **77,** 382 (1988).
10. A. Knuttel and R. Kimmich, Double-quantum filtered volume-selective NMR spectroscopy, *Magn. Reson. Med.* **10,** 404 (1989).
11. G. C. McKinnon and P. Boesiger, A one-shot lactate-editing sequence for localized whole-body spectroscopy, *Magn. Reson. Med.* **8,** 355 (1988).
12. S. Crozier, I. M. Brereton, S. E. Rose, J. Field, G. F. Shannon, and D. M. Doddrell, Application of volume-selected, two-dimensional multiple-quantum editing in vivo to observe cerebral metabolites, *Magn. Reson. Med.* **16,** 496 (1990).
13. M. A. Thomas, H. P. Hetherington, D. J. Meyerhoff, and D. B. Twieg, Localized double-quantum-filtered ^{1}H NMR spectroscopy, *J. Magn. Reson.* **93,** 485 (1991).
14. H. Lei and J. Peeling, Multiple-voxel double-quantum lactate edited spectroscopy using two dimensional longitudinal Hadamard encoding, *Magn. Reson. Med.* **42,** 19 (1999).
15. L. Jouvensal, P. G. Carlier, and G. Bloch, Practical implementation of single-voxel double-quantum editing on a whole-body NMR spectrometer: Localized monitoring of lactate in the human leg during and after exercise, *Magn. Reson. Med.* **36,** 487 (1996).
16. J. R. Keltner, L. L. Wald, B. D. Frederick, and P. F. Renshaw, In vivo detection of GABA in human brain using a localized double-quantum filter technique, *Magn. Reson. Med.* **37,** 366 (1997).
17. J. R. Keltner, L. L. Wald, P. J. Ledden, Y. C. Chen, R. T. Matthews, E. H. Kuestermann, J. R. Baker, B. R. Rosen, and B. G. Jenkins, A localized double-quantum filter for the in vivo detection of brain glucose, *Magn. Reson. Med.* **39,** 651 (1998).
18. A. H. Trabesinger, O. M. Weber, C. O. Duc, and P. Boesiger, Detection of glutathione in the human brain in vivo by means of double quantum coherence filtering, *Magn. Reson. Med.* **42,** 283 (1999).
19. R. B. Thompson and P. S. Allen, A new multiple quantum filter design procedure for use on strongly coupled spin systems found in vivo: Its application to glutamate, *Magn. Reson. Med.* **39,** 762 (1998).
20. G. McKinnon and P. Boesiger, Lactate signal loss with echo based volume selective spectroscopy, *Magn. Reson. Med. Biol.* **4,** 101 (1990).
21. M. Bunse, W. I. Jung, and O. Lutz, Localized double spin echo spectroscopy of weakly homonuclear coupled spin systems: Influence of chemical shift artifacts, *Appl. Magn. Reson.* **3,** 185 (1992).
22. F. Schick, T. Nagele, U. Klose, and O. Lutz, Lactate quantification by means of PRESS spectroscopy—Influence of refocusing pulses and timing scheme, *Magn. Reson. Imaging* **13,** 309 (1995).
23. D. A. Yablonskiy, J. J. Neil, M. E. Raichle, and J. J. Ackerman, Homonuclear *J* coupling effects in volume localized NMR spectroscopy: Pitfalls and solutions, *Magn. Reson. Med.* **39,** 169 (1998).
24. H. Lei and J. Peeling, Off-resonance effects of the radiofrequency pulses used in spectral editing with double quantum coherence transfer, *J. Magn. Reson.* **144,** 89 (2000).
25. T. T. Nakashima and R. E. D. McClung, Simulation of two-dimensional NMR spectra using product operators in the spherical basis, *J. Magn. Reson.* **70,** 187 (1986).
26. P. B. Kingsley, Scalar coupling and zero-quantum coherence relaxation in STEAM: Implications for spectral editing of lactate, *Magn. Reson. Med.* **31,** 315 (1994).
27. H. Lei and J. Peeling, A localized double quantum filter for in vivo detection of taurine, *Magn. Reson. Med.* **42,** 454 (1999).
28. L. A. Trimble, J. F. Shen, A. H. Wilman, and P. S. Allen, Lactate editing by means of selective-pulse filtering of both zero- and double-quantum coherence signals, *J. Magn. Reson.* **86,** 191 (1990).
29. J. Slotboom, A. F. Mehlkopf, and W. M. Bovee, The effects of frequency-selective RF pulses on *J*-coupled spin-1/2 systems, *J. Magn. Reson. A* **108,** 38 (1994).